Supplemental Information:
Behavior and Mechanics of Dense Microgel Suspensions

Svetoslav Nikolov[†], Alberto Fernandez-Nieves[‡, §, ⊥], Alexander Alexeev[*, †]

[†]George W. Woodruff School of Mechanical Engineering and [‡]School of Physics, Georgia Institute of Technology, Atlanta, Georgia, 30332, United States

[§]Department of Condensed Matter Physics, University of Barcelona, 08028 Barcelona, Spain

[⊥]ICREA-Institucio Catalana de Recerca i Estudis Avancats, 08010 Barcelona, Spain

Email: alexander.alexeev@me.gatech.edu.

We utilize dissipative particle dynamics (DPD) to model microgel suspensions. DPD is a mesoscale particle-based method in which beads represent clusters of molecules and interact via soft and pairwise potentials (1). In DPD, three types of forces act between a given bead i and each of its neighbors j within a cutoff radius r_C. The total interaction force $\boldsymbol{F} = \sum_{j \neq i}\left(\boldsymbol{F}_{ij}^{C} + \boldsymbol{F}_{ij}^{D} + \boldsymbol{F}_{ij}^{R}\right)$, where, $\boldsymbol{F}_{ij}^{C} = a_{ij}\, w\left(r_{ij}\right)\hat{\boldsymbol{r}}_{ij}$ is a conservative repulsive force accounting for the excluded volume interaction between beads, a_{ij} is the strength of the repulsive potential between beads i and j, $\boldsymbol{F}_{ij}^{D} = -\gamma w\left(r_{ij}\right)^{2}\left(r_{ij} \cdot v_{ij}\right)\hat{\boldsymbol{r}}_{ij}$ is a dissipative force, that mimics the effects of viscosity, and $\boldsymbol{F}_{ij}^{R} = \sigma w\left(r_{ij}\right)\xi_{ij}(\Delta t)^{-1/2}\,\hat{\boldsymbol{r}}_{ij}$ is a random force, accounting for the presence of thermal fluctuations. According to the fluctuation-dissipation theorem, the dissipative and random forces are coupled by $\sigma^2 = 2\gamma k_B T$ (1). In addition, $w\left(r_{ij}\right) = 1 - \tilde{r}_{ij}$ is a weighing function with $\tilde{r}_{ij} = r_{ij} \,/\, r_C$ and $r_{ij} = \left|\boldsymbol{r}_i - \boldsymbol{r}_j\right|$ is the center-to-center distance between beads i and j. Moreover, $\hat{\boldsymbol{r}}_{ij} = \left(\boldsymbol{r}_i - \boldsymbol{r}_j\right) \,/\, r_{ij}$, $\xi_{ij}(\Delta t)$ is a variable that is randomly drawn from a Gaussian distribution with zero mean and unit variance, k_B is the Boltzmann constant, and T is the absolute temperature. In our simulations, we set $r_C = 1$, $\gamma = 4.5$, $k_B T = 1$, and take the bead mass to be $m = 1$ (2). The integration time step is set to $\Delta t = 0.01$. We express all dimensional parameters in DPD units, unless indicated otherwise.

Microgels are assembled from polymer chains with monomers interacting via bond, angle, and segmented-repulsive potentials. The bond potential energy, which sets the extensibility of a chain, is $U_{bond} = k_{bond}\left(r - r_{eq}\right)^{2}$, with k_{bond} the bond stiffness and r_{eq} the equilibrium separation length between monomer beads. The angle potential energy, which defines the persistence length of a chain, is given by $U_{bend} = k_{bend}(1 + cos\,\theta)$, with k_{bend} the bending stiffness and θ the angle between two monomer bonds sharing a common bead. The segmented repulsive potential prevents polymer chains from crossing each other. It is given by $\boldsymbol{F}_{ij}{}^{SRP} = C\left(1 - r_{min}/r_{c_{SRP}}\right)\hat{\boldsymbol{r}}_{ij}$, where $r_{c_{SRP}}$ is the cutoff distance, r_{min} is the minimum distance between two bonds, and C is the strength of the potential (3). Following our previous work (1), we set $r_{c_{SRP}} = 0.5$, $C = 100$, $k_{bond} = 35$, $r_{eq} = 0.6$, and $k_{bend} = 5$. All simulations are carried out using the LAMMPS software (4).

To evaluate microgel properties such as interpenetration, deformation, and shrinking/swelling within the suspension we create surface meshes around each microgel particle. Each surface mesh is created using the alpha-shape algorithm developed by Edelsbrunner and Mücke (5), which initially creates a Delaunay tessellation based on the coordinates of each DPD polymer particle. The specified probe radius or alpha parameter is used to determine whether the tessellated simplices are part of the final microgel mesh. The implementation procedure of this algorithm is outlined by Stukowski (6). The generated surface meshes are constructed using a probe with a radius of about 2/3 of the average crosslink spacing. Such probe size in our case corresponds to approximately 0.45 of the contour length of chains. The crosslinking distance and chain length are evaluated after the equilibration in good solvent. On the one hand, we find that the use of smaller probe radii can lead to disconnected and segmented meshes. On the other hand, a larger probe radius does not capture minute changes in volume. Surface meshing is done using the OVITO software (7), where internal voids in the mesh are removed (8, 9). Figure S1 shows a rendering of the surface mesh and the corresponding microgel particle. The surface mesh is semi-transparent and colored in blue.

www.pnas.org/cgi/doi/10.1073/pnas.2008076117

We obtain the radial density profile by creating a series of radial shells (with thickness $\Delta r = 0.2$ distance units) around the particle center of mass which span from $r = \Delta r$ to $r = 1.5R$; the values of R are given in Table 1. By tracking the quantity of polymer in each shell we can determine how the density of each microgel varies radially. Radial density measurements are taken when the microgels are in equilibrium with the solvent. Radial density measurements for each particle are done every 5,000 timesteps over the course of 100,000 timesteps. The average radial density is shown in Figure S2 for microgels I-IV. As can be seen for microgels I and II with a uniform crosslink distribution, the radial density is constant up to $r \approx 3/4\,R$. The fact that the polymer density does not remain constant for larger r, can be attributed to the random crosslink distribution coupled to the small microgel size, which is 6-10 mesh sizes in diameter; it is thus the loose character of the microgels that causes the polymer density to decrease near the gel-solvent interphase. In contrast, for microgels III and IV, which have a Gaussian crosslink distribution, the core region, where the density is constant, exists only up to approximately $r \approx 1/5\,R$. Hence, the corona region, corresponding to the region where the density clearly decreases, is roughly 3.5 times larger for microgels with a Gaussian crosslink distribution compared to microgels with a uniform crosslink distribution. All of them nevertheless exhibit the common core-corona structure found for many experimental microgels.

The chain length distribution of microgels I-IV is shown in Figure S3. The figure shows that although the average chain length for microgels I, III, and IV is similar, microgel IV has a much wider chain length distribution, ~70% of mean, compared to microgels I and III, which have a distribution width that is ~14% of the mean. In addition, microgel II has a mean chain length of ~21; this is nearly twice the mean chain length of the other three microgels. The width of the chain length distribution for microgel II is similar to that of microgels I and III, and is also ~14% of the mean.

We define the generalized packing fraction as $\zeta = \kappa V_{eq}/V_{sus}$. Here κ is the number of microgel particles in the suspension, V_{eq} is the equilibrium volume of a standalone microgel particle at the given solvent condition, and V_{sus} is the volume of the suspension. We alter the generalized packing fraction by either changing V_{sus} (volumetric method) or V_{eq} (solvency method). The changes in V_{sus} are achieved in good solvent conditions via compression whereas the changes in V_{eq} are realized by varying the microgel-solvent interactions. Swelling curves for microgels I-IV are shown in Figure S4. From the figure, we find that the lower critical solution value of a_{P-S}, corresponding to the lower critical solution temperature of experimental microgels, is approximately 29. We also find that the swelling ratio is approximately 10.

In the volumetric method, we initially replicate each microgel particle $\kappa = 106$ times in a cubic simulation box with dimensions $300 \times 300 \times 300$ and fill the remaining space with solvent. Initially the microgel particles are frozen and the solvent is allowed to equilibrate around the microgels (100,000 timesteps). After this, the microgel dynamics is turned on and the microgel particles are allowed to equilibrate with the external solvent (200,000 timesteps). To change ζ we compress the computational box in 0.2 increments per 10,000 timesteps along each dimension, at constant a_{P-S}. Once the required packing fraction is obtained (the target box sizes are listed in Table S1), the suspension is equilibrated so that the pressure is constant with time, which usually takes approximately 500,000 timesteps. Generally, the number of microgel particles in the suspension is set to $\kappa = 106$, except in two cases where to reduce computational costs κ was decreased (see Tables S1 and S2). In these cases, κ was decreased by removing microgel particles from the suspension and replacing them with extra solvent. For each of these cases the equilibration process again involved running the dynamics until the pressure in the suspension is constant with time. The total DPD bead density is always kept constant and equal to $\rho = 3$ (1).

For the solvency method, we keep the box size V_{sus} constant and change V_{eq} by varying the polymer-solvent repulsion parameter a_{P-S} in the range between 25 and 35. After changing a_{P-S} each suspension is equilibrated for approximately 500,000 timesteps, until the internal pressure in the suspension is constant with time.

To measure the bulk modulus, we start from an equilibrated state and compress the simulation box 5 times in 0.2% increments every 50,000 timesteps. The suspension bulk modulus is obtained as an average of these 5 measurements. The single-microgel bulk modulus K_p is measured by placing the microgel inside a semi-permeable shell which restricts the polymer network but allows solvent to freely pass. By varying the radius of the shell, we compress the network mimicking changes in the osmotic

pressure, as outlined in our earlier work (1). The single-microgel modulus K_p is measured at the average microgel volume in the suspension at the given solvency a_{P-S}. This approach matches the experimental procedure in ref. (10). Figure S5 shows the behavior of the single-microgel modulus at approximate suspension conditions. As shown by the light and dark green triangles in the figure, the increases in ζ_0 cause the microgel bulk modulus to increase in good solvent. Meanwhile, for a fixed ζ_0, microgel IV has the lowest K_P in good solvent, most likely due to the large dangling loose chains near the microgel periphery, which are attributed to both the Gaussian crosslinking structure and the wide chain length distribution.

To establish how our microgel model is capable of reproducing relevant mechanic and kinetic behavior of experimental microgels, we compare our model to experimentally validated theories. Specifically, we match the response of our microgels with the well-established theories of Flory-Rehner (11) and Tanaka (12), as shown in Figures S6 and S7, respectively. The fitting parameters associated with both theories are presented in Table S3. We emphasize that these theories are known to describe experimental behavior. We use the agreement between our simulations and the theories as a benchmark to affirm that our computational models properly capture relevant experimental behavior. We further note that these theories pertain to different aspects of microgel behavior: while the theory of Flory-Rehner describes the equilibrium swelling behavior, the theory of Tanaka describes swelling kinetics and thus pertains to the dynamic behavior.

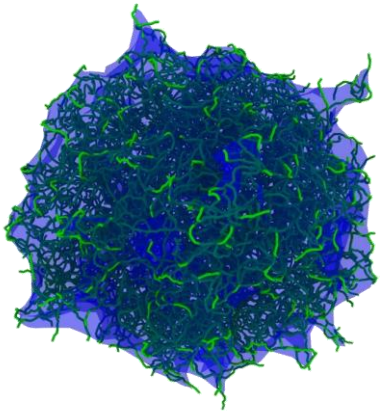

Figure S1. Surface mesh of an example DPD microgel particle. The mesh is colored in blue and is transparent. The microgel is shown in green.

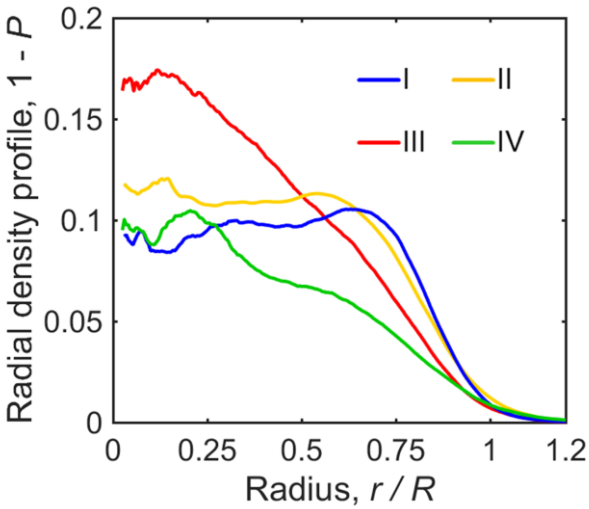

Figure S2. Radial density profiles for microgels I-IV. Microgels I and II have a uniform crosslink distribution and have an approximately constant crosslink density throughout the microgel domain. For these microgels the density decreases near the gel-solvent interphase. This can be attributed to the random distribution of crosslinking sites. For microgels III and IV, the radial density is constant only near the particle center, which then defines the microgel core. The corona region, where the density decreases, spans the range $1/5\,R < r < R$.

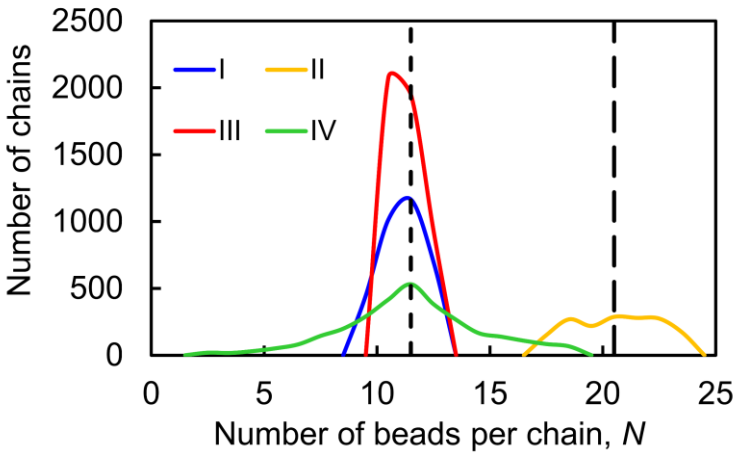

Figure S3. Chain length distribution for microgels I-IV. Microgels I, III, and IV have on average 12 beads per chain. Meanwhile, microgel II has on average 21 beads per chain. The width of the chain length distribution for microgels I and III is nearly identical. Microgel IV has a much wider chain length distribution than the other 3 microgels.

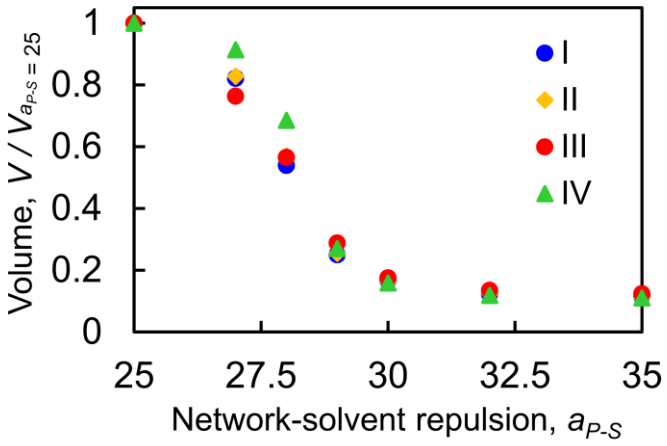

Figure S4. Swelling curves for microgels I-IV.

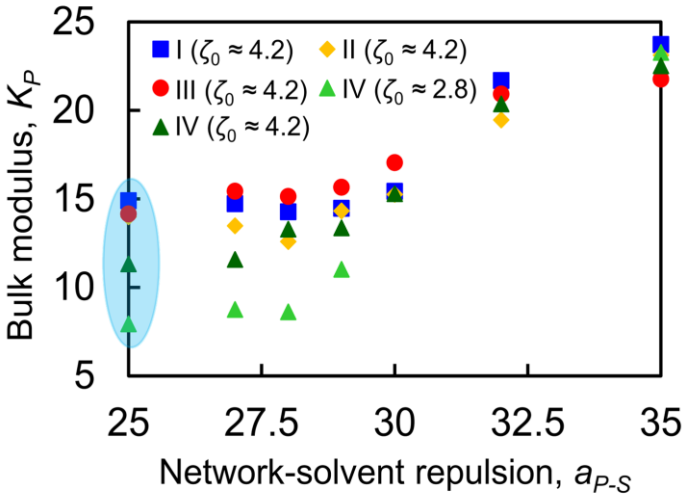

Figure S5. Single-microgel bulk modulus at the specified solvency and generalized packing fraction. The light blue semi-transparent region highlights the data which was used to normalize the suspension bulk moduli in the volumetric method. Microgel IV which has a wider chain length distribution is softer in the good solvent. In the bad solvent, all microgels reach a nearly identical deswollen state and, hence, attain similar bulk moduli.

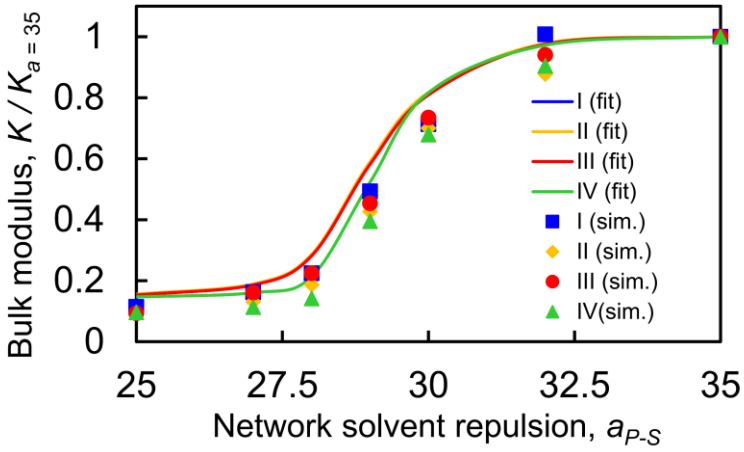

Figure S6. Comparison of bulk modulus data with Flory-Rehner theory. The fits follow the procedure outlined in our previous work (1). Resulting fitting parameters for the bulk modulus fits are listed in Table S3. In all cases, the theoretical fits match the computational data well.

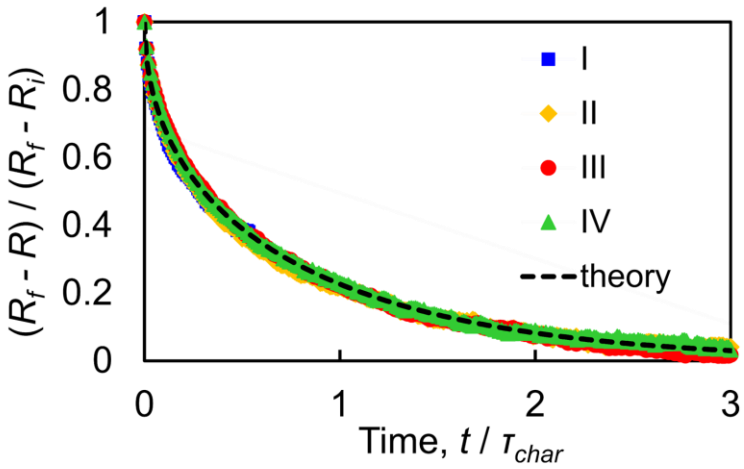

Figure S7. Comparison of swelling kinetics for microgels I-IV with Tanaka's theory. In these simulations, initially swollen microgels ($a_{P-S} = 25$) are exposed to bad solvent ($a_{P-S} = 35$) at time $t = 0$. The values of τ_{char} are reported in Table S3. Close agreement is found between the theory and the simulation results. Note that the marks for different microgels overlap.

Table S1. Simulation box length L ($V_{sus} = L^3$) for all suspensions in the volumetric method at which measurements are taken. The cells marked in green were also examined using $\kappa = 16, 26,$ and 46. All other cells were studied with $\kappa = 106$.

	Simulations			
	I ($a_{P\text{-}S}$ = 25)	II ($a_{P\text{-}S}$ = 25)	III ($a_{P\text{-}S}$ = 25)	IV ($a_{P\text{-}S}$ = 25)
Box lengths, L (ζ)	300 (0.39)	230 (0.15 0.25, 0.43, 1.0)	276 (0.68)	265 (0.62)
	276 (0.50)	210 (1.32)	266 (0.76)	226 (0.15, 0.25, 0.43, 1.0)
	264 (0.57)	190 (1.78)	257 (0.84)	180 (1.98)
	250 (0.68)	180 (2.09)	245 (0.97)	170 (2.35)
	224 (0.94)	160 (2.98)	233 (1.13)	160 (2.82)
	175 (1.96)	150 (3.61)	197 (1.87)	150 (3.42)
	155 (2.90)	139 (4.54)	173 (2.76)	140 (4.21)
	135 (4.27)	128 (5.81)	162 (3.37)	
	125 (5.37)		149 (4.33)	
			137 (5.57)	

Table S2. Simulation box length L ($V_{sus} = L^3$) for all suspensions in the solvency method at which measurements were taken.

Simulations	Box lengths, L (ζ)
I ($\zeta_0 \approx 4.2$)	135 (4.27, 3.52, 2.36, 1.05, 0.73, 0.61, 0.53, 0.49)
II ($\zeta_0 \approx 4.2$)	139 (4.54, 3.46, 2.39, 1.08, 0.69, 0.52, 0.47)
III ($\zeta_0 \approx 4.2$)	149 (4.33, 3.28, 2.43, 1.24, 0.75, 0.58, 0.53)
IV ($\zeta_0 \approx 2.8$)	161 (2.82, 2.58, 1.91, 0.79, 0.44, 0.34, 0.30)
IV ($\zeta_0 \approx 4.2$)	141 (4.21, 3.79, 2.84, 1.13, 0.66, 0.50, 0.46)

Table S3. Fitting parameters for the bulk modulus and kinetics fits

Microgel	k_bT / v_s	N_cv_s / V_0	χ_0	χ_1	χ_2	τ_{char}
I	2.15e-21	2.48E+22	0.5099	0.0496	0.5012	1200
II	2.13e-21	2.50E+22	0.4979	0.0502	0.5021	1000
III	2.50e-21	3.10E+22	0.5009	0.0497	0.5026	950
IV	1.93e-21	2.69E+22	0.5148	0.05	0.4993	930

REFERENCES

1. Nikolov S, Fernandez-Nieves A, Alexeev A (2018) Mesoscale modeling of microgel mechanics and kinetics through the swelling transition. *Applied Mathematics and Mechanics* 39:47-62.
2. Groot RD, Warren PB (1997) Dissipative particle dynamics: Bridging the gap between atomistic and mesoscopic simulation. *J Chem Phys* 107:4423-4435.
3. Sirk TW, Slizoberg YR, Brennan JK, Lisal M, Andzelm JW (2012) An enhanced entangled polymer model for dissipative particle dynamics. *J Chem Phys* 136:134903.
4. Plimpton S (1995) Fast parallel algorithms for short-range molecular dynamics. *Journal of Computational Physics* 117:1-19.
5. Edelsbrunner H, Mücke EP (1994) Three-dimensional alpha shapes. *ACM Transactions on Graphics (TOG)* 13:43-72.
6. Stukowski A (2014) Computational analysis methods in atomistic modeling of crystals. *JOM* 66:399-407.
7. Stukowski A (2009) Visualization and analysis of atomistic simulation data with OVITO–the Open Visualization Tool. *Model Simul Mater Sc* 18:015012.
8. Ahrens J, Geveci B, Law C (2005) Paraview: an end-user tool for large data visualization. *The Visualization Handbook* 717.
9. Ayachit U (2015) *The paraview guide: a parallel visualization application* (Kitware, Inc.).
10. Liétor-Santos JJ, Sierra-Martín B, Fernández-Nieves A (2011) Bulk and shear moduli of compressed microgel suspensions. *Physical Review E* 84:060402.
11. Flory PJ (1953) *Principles of polymer chemistry* (Cornell University Press).
12. Tanaka T, Fillmore DJ (1979) Kinetics of swelling of gels. *The Journal of Chemical Physics* 70:1214-1218.